Hydrostatic pressure effects on hydrogen permeation in A514 steel during galvanostatic hydrogen charging

X.L. Xiong [a], X. Tao [a], Q.J. Zhou [b], J.X. Li [a], Alex A. Volinsky [c], Y.J. Su [a],*

[a] Corrosion and Protection Center, Key Laboratory for Environmental Fracture (MOE), University of Science and Technology Beijing, Beijing 100083, China
[b] Research Institute, Baoshan Iron & Steel Co. Ltd., Shanghai 201900, China
[c] Department of Mechanical Engineering, University of South Florida, Tampa, FL 33620, USA

ARTICLE INFO

ABSTRACT

A514 offshore structural steel was exposed to hydrostatic pressure ranging from 0.1 to 40 MPa to examine hydrogen permeation during galvanostatic hydrogen charging. Hydrostatic pressure decreases the energy barrier for hydrogen absorption and desorption, while increasing hydrogen adsorption. These effects are induced by both steady-state current density and the apparent diffusivity slight increase with hydrostatic pressure. Taking surface effect of hydrogen permeation into account, the intrinsic diffusivity of $(3.2 \pm 0.04) \times 10^{-6}$ cm^2/s is obtained, which is independent of the hydrostatic pressure.

© 2016 Elsevier Ltd. All rights reserved.

1. Introduction

Duplex stainless steel is widely used in deep sea engineering due to its combination of high strength and high resistance to pitting corrosion and chloride stress corrosion cracking. However, hydrogen induced-cracking (HIC) has been observed in duplex steel pipes when submerged in deep sea environment. Taylor et al. reported that HIC occurred in super duplex hub forging containing welded pipe connection in the BP Amoco Foinaven Field after only 6 months of service [1]. Hydrogen damage can be caused by both metal structure [2–5] and environmental factors [6,7]. The cathodic protection potential is an important factor of hydrogen damage. Woollin et al. [8] and Du [9] observed that the sensitivity of the HIC increased as the cathodic protection potential decreased, based on the constant load, pre-cracked bending and the slow strain rate tests under different cathodic protection potentials. Olsen et al. proved that hydrostatic pressure could cause a significant increase in hydrogen concentration of super martensitic stainless and duplex stainless steels when immersed in 3.5% NaCl electrolyte with aluminium anodes, which is the reason why HIC occurs in deep sea environment [10]. Thus, studying the mechanism of hydrogen diffusion in metal under different hydrostatic pressure is very important for simulating the hydrostatic pressure effects on hydrogen permeation in metals.

Experiments on hydrogen permeation under hydrostatic pressure have been carried out since 1966. Woodward et al. measured hydrogen permeation in high strength steel under different hydrostatic pressures with potentiostatic hydrogen charging. They found that hydrogen permeation rate was considerably higher at 100 bar than at 1 bar [11]. Similar results were obtained in the Nanis's experiment, where diffusivity remained the same for different hydrostatic pressures [12]. However, Smirnova et al. found that permeation rates for the UNS S4 1000 stainless steel were the same at 1–100 bar when electrolyte at the entry side was stirred [13]. Blundy and Sheer also found that when the electrolyte at the entry side was stirred, the permeation rate for different hydrostatic pressures was the same. They hypothesized that the permeation rate increased with the partial pressure of hydrogen at the entry side and that the hydrostatic pressure did not directly affect the permeation rate [14,15].

Mentioned studies of hydrostatic pressure effects on hydrogen permeation used the classic model to fit the experimental data [11–15], which only considered hydrogen diffusion in the bulk, while surface effects have not been taken into account. Hydrogen solubility in electrolyte increases with hydrostatic pressure [16]. For 10 MPa hydrostatic pressure, hydrogen produced by hydrogen evolution reaction during 1 h with 5 mA/cm^2 hydrogen charging current density completely dissolved in the electrolyte and gathered near the entry side of the membrane, which could restrain adsorbed hydrogen atoms combining into H$_2$ molecules. It is reasonable to assume that this phenomenon increases the amount of adsorbed hydrogen atoms. Thus, higher hydrostatic pressure causes

---

greater subsurface coverage of hydrogen beneath the entry side, induced by the steady-state current density increase with hydrostatic pressure.

The purpose of this work is to quantify the influence of surface hydrogen absorption and desorption on hydrogen diffusivity under different hydrostatic pressure. The effects of the hydrostatic pressure, membrane thickness and Ni coating on hydrogen permeation behaviour were characterized. Taking surface effects of hydrogen permeation into account, the intrinsic diffusivity is obtained, which is independent of the hydrostatic pressure.

2. Hydrogen permeation theories

The Devanathan and Stachurski double cell electrochemical permeation model [17] is the classic model used to study hydrogen diffusion in metals, which is based on the Fick's second law:

$$\frac{\partial C}{\partial t} = D \frac{\partial^2 C}{\partial x^2} \tag{1}$$

In the classic hydrogen permeation model, permeation current build-up transient $J = f(t)$ is recorded when constant potential or constant current is applied at the entry side. In most cases, hydrogen exit side is coated with a thin palladium or nickel layer to achieve full oxidation of hydrogen. It is generally assumed that the diffusion process of hydrogen into the bulk metal is a rate-determining step and that the output concentration is zero. Here, ideal hydrogen permeation boundary conditions can be given by:

$$t = 0, C(x, 0) = 0$$

$$t > 0, C(0, t) = C_0, C(L, t) = 0 \tag{2}$$

By solving the Fick's second law for ideal hydrogen permeation boundary conditions, one arrives at:

$$\frac{J}{J_\infty} = \frac{2L}{\sqrt{\pi Dt}} \sum_{n=0}^{\infty} \exp\left(-\frac{(2n+1)^2 L^2}{4Dt}\right) \tag{3}$$

Here, J is the measured permeation rate at time t, J_∞ is the steady-state permeation rate ($t \to \infty$), D is the diffusivity, and L is the specimen thickness.

Classic model is most widely used in hydrogen permeation to obtain diffusivity. However, many researchers have observed that there is scatter of several orders of magnitude in the evaluation of iron diffusivity using the classic model when the membrane thickness is varied [17–19]. This is due to hydrogen trapping in metal defects, which can contribute to discrepancies in the evaluation of the diffusion coefficient [20–22]. Moreover, surface effects are present at the entry side, limiting the permeation rate. The surface effect is related to the specimen thickness in the double cell electrochemical permeation experiments. This relationship has been the subject of many studies [18,23–26] with increasingly lower apparent hydrogen diffusivity obtained for iron and steel membranes of progressively decreasing thickness. Wach et al. [23] claimed that the formation of a barrier at the entry side of the membranes induced an error in the diffusivity values. Equivalent thickness should be considered to correct this value.

To study the surface effect on hydrogen permeation, Wang [27] put forward a model for hydrogen permeation by charging with hydrogen gas, which considered hydrogen adsorption and desorption, to illustrate the deviation of the Siverts' law under low hydrogen pressure. Based on the Wang's model, thermodynamic model for hydrogen permeation was proposed by Zhang et al. to evaluate hydrogen diffusivity, considering both absorption and desorption processes [18]. From the Wang's model, the continuity of the flux at the entry side requires:

$$k_1^+ P_1 - k_1^- C = -D \frac{\partial C}{\partial x}, x = 0 \tag{4}$$

Here, k_1^+ and k_1^- are the rate parameters for hydrogen adsorption and desorption reactions, respectively. The variable P_1 is hydrogen pressure in the gas phase. The variable C is hydrogen concentration.

In the same way, boundary conditions at the exit side are given by:

$$k_2^- C - k_2^+ P_2 = -D \frac{\partial C}{\partial x}, x = L \tag{5}$$

Here, k_2^+ and k_2^- are rate parameters for hydrogen adsorption and desorption reactions, respectively. The variable P_2 is hydrogen pressure in the gas phase. Generally, a membrane has the same energy barrier at both sides. Therefore, for simplicity, Zhang et al. assumed that $k_1^- = k_2^- = k$, which means that the desorption rate depends on the surface conditions, and that $k_1^+ P_1 = k_p$, which is the absorption parameter. It denotes the forward flux of hydrogen from the gas phase into the sample at the entry side and therefore is related to gas pressure or charging current density in electrochemical tests. Usually, the value of $P_2 = 0$ is used in an electrochemical permeation test.

With the boundary conditions mentioned above, an analytical solution of the Fick's second law is:

$$C = -\frac{k_p}{2D + kL} x + \frac{k_p(D + kL)}{2kD + k^2 L} - \sum_{m=1}^{\infty} A_m e^{-D\lambda_m^2 t} [D\lambda_m \cos(\lambda_m x) + k \sin(\lambda_m x)]$$

$$A_m = \frac{2k_p}{\lambda_m \left[\left(D^2 \lambda_m^2 + k^2\right) L + 2kD\right]} \tag{6}$$

Both diffusivity and desorption rates are evaluated by fitting the entire normalized permeation curve with the following equation:

$$\frac{J}{J_\infty} = 1 + 2(2D + kL) \sum_{m=1}^{\infty} \frac{[k\cos(\lambda_m L) - D\lambda_m \sin(\lambda_m L)] e^{-D\lambda_m t}}{\left[\left(D^2 \lambda_m^2 + k^2\right) L + 2kD\right]} \tag{7}$$

where λ_m is the mth positive root of $\tan(\lambda_m L) = \frac{2kD\lambda_m}{D^2 \lambda_m^2 - k^2}$.

The drift velocity through the surface, V_s, and drift velocity in the bulk, V_b, are introduced as:

$$V_s = k, \quad V_b = \frac{D}{L}. \tag{8}$$

Then, the permeation rate at steady state J_∞ can be expressed in terms of the ratio of the drift velocities and the absorption parameter, k_p:

$$J_\infty = \frac{k_p}{2 + V_s/V_b} \tag{9}$$

After evaluating the diffusivity and the desorption rate, the absorption parameter is calculated using Eq. (9). Then, the permeation concentration C_0 is determined from:

$$C_0 = \frac{k_p}{k} \tag{10}$$

Finally, the concentrations at the entry and exit sides for steady state can be evaluated using the following equations:

$$\frac{C_{entry}}{C_0} = \frac{1 + V_s/V_b}{2 + V_s/V_b}, \quad \frac{C_{exit}}{C_0} = \frac{1}{2 + V_s/V_b} \tag{11}$$

Since the absorption, desorption and diffusion are all expressed in the above model, it is possible to measure the effects of hydrostatic pressure on these reactions using the Zhang's model.
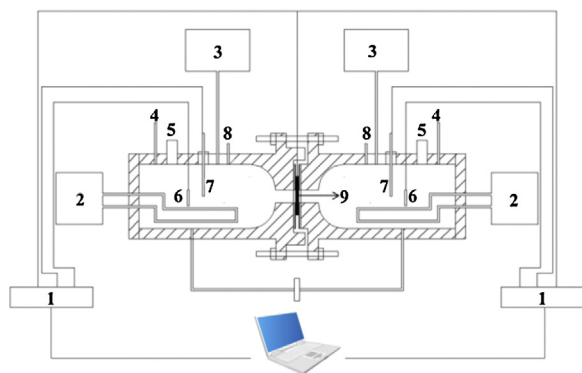
Fig. 1. Schematic of the diffusion test equipment: (1) Electrochemical workstation, (2) Thermostat controller, (3) Plunger metering pump, (4) Safety valve, (5) Pressure monitors, (6) Counter electrode, (7) Reference electrode, (8) Liquid outlet, (9) Specimen.

3. Experimental procedure

3.1. Specimens preparation

A514 offshore structural steel is used in the present study. The composition of the material is as follows (wt%): 0.2 C, 0.78 Mn, 0.49 Cr, 0.20 Mo, 0.049 V, 0.0006 B, 0.0080 P, 0.006 S, and 0.020 Ti. The permeation specimens are cylindrical with 4 cm diameter and the circular area exposed to the solution is 1.2 cm in diameter, so that the edge effects would be minimized to ensure the one-dimensional model validity.

Three specimen groups were adopted to vary the effects of absorption and desorption processes to study the effects of hydrostatic pressure, thickness and nickel coating on hydrogen permeation. Group I specimens were polished on both sides, and hydrogen exit side was coated with 100 nm of nickel using a sputter deposition process in an ultra-high vacuum to restrain hydrogen atoms from recombining to hydrogen molecules at the exit side. Ni coating significantly increases the oxidation reaction at the exit surface and consequently reduces the non-measured fraction of the oxidation electric current to a negligible value. Another important reason for the Ni coating is that without it an oxide layer can form on the specimen surface acting as a diffusion barrier. All sputter deposition processes were conducted in a thin film sputtering system (LAD18, KJLC). The specimens were 1.1 ± 0.01 mm thick. Group II specimens were polished on both sides, and only one side was coated with 100 nm of nickel. These specimens have a thickness of approximately 0.5 ± 0.01 mm. Group III specimens were polished on both sides, and two sides were coated with 100 nm of nickel. These specimens have a thickness of approximately 0.5 ± 0.01 mm.

3.2. High pressure electrochemical hydrogen permeation equipment

The electrochemical hydrogen permeation equipment used in this study was developed by the Environmental Fracture Laboratory at the University of Science and Technology Beijing and can be used to study variations in hydrogen permeation and diffusion as functions of temperature and hydrostatic pressure. The schematic diagram of the equipment is shown in Fig. 1, which consists of a two compartment autoclave integrated with hydraulic and temperature control systems. Temperature in the autoclaves can be controlled in the 0–40 °C range. Electrolyte in the autoclaves can be pressurised to a maximum hydrostatic pressure of 40 MPa via a solution supplied from an external tank.

3.3. Electrochemical hydrogen permeation tests

A specimen in the form of a thin membrane separates two electrically isolated electrochemical cells. A solution of 0.2 mol/L NaOH was poured into each cell. In the hydrogen charging cell, low charging current density of 5 mA/cm^2 was used in the permeation tests. Hydrogen atoms were produced and adsorbed onto the specimen surface, some of which were absorbed and diffused through the material. In the other cell (oxidation cell), a positive potential (+300 mV vs. Ag/AgCl) was applied to the opposite surface of the specimen by an electrochemical workstation (Interface 1000, Gamry). Hydrogen that reached the surface by diffusion through the specimen was immediately oxidized, and hydrogen current was measured.

Traps have a significant influence on hydrogen diffusivity in metals [20,22,28]. Specifically, Kim pointed out that the trap density during the first time permeation was twice as much as the second permeation [29]. To ensure the reliability and repeatability of the experimental data, hydrogen charging was carried out first to fill the traps under atmospheric pressure, and then all of the charged specimens were exposed to air for 48 h to completely release diffusible hydrogen atoms in the lattice. Finally, hydrogen permeation experiments were performed under different hydrostatic pressures.

4. Results and discussion

The permeation curves for the three group specimens for different hydrostatic pressures at 25 °C are shown in Fig. 2(a)–(d). As seen in Fig. 2(a), the permeation curves for the specimens with a thickness of approximately 1.1 mm show no regular changes with different hydrostatic pressures. However, the permeation current density clearly increases with hydrostatic pressure in Fig. 2(c) and (d) when the specimen thickness is 0.5 mm.

Steady-state current density i_∞, intrinsic diffusivity D, desorption rate k, absorption parameter k_p, permeation concentration C_0 and hydrogen concentration on both sides of the membranes, i.e., C_{entry} and C_{exit} from the Zhang's model, and apparent diffusivity D_c from the classic model, were calculated based on the permeation curves and are listed in Table 1 for the three groups.

Variations in the steady-state current density i_∞, diffusivities D and D_c, desorption rate k, absorption parameter k_p and the permeation concentration C_0 as functions of the hydrostatic pressure are shown in Fig. 3(a)–(e), respectively.

4.1. Effect of hydrostatic pressure on the steady-state current density

Fig. 3(a) indicates that the effect of hydrostatic pressure on i_∞ depends on the thickness of the specimen. For the 1.1 mm thick specimens, i_∞ is almost independent of the hydrostatic pressure. However, for the 0.5 mm specimens, i_∞ increases with hydrostatic pressure. To date, there has been no mention of the sample thickness influencing the relationship between hydrostatic pressure and i_∞. For a 1 mm thick specimen, Nanis showed that i_∞ increased with hydrostatic pressure [12]. However, Blundy reported that i_∞ was almost independent of the hydrostatic pressure when stirring the electrolyte at the entry side [14]. For a specimen less than 0.5 mm thick, Woodward [11] indicated that i_∞ increased with hydrostatic pressure, but Blundy [15] and Smirnova [13] showed that i_∞ was independent of hydrostatic pressure.

The reason why hydrostatic pressure increases the steady-state current density i_∞ for the thin samples is as follows. Based on Eq. (9), $i_\infty = k_p F / (2 + kl/D)$, where D is independent of hydrostatic pressure, while the adsorption parameter k_p and desorption rate
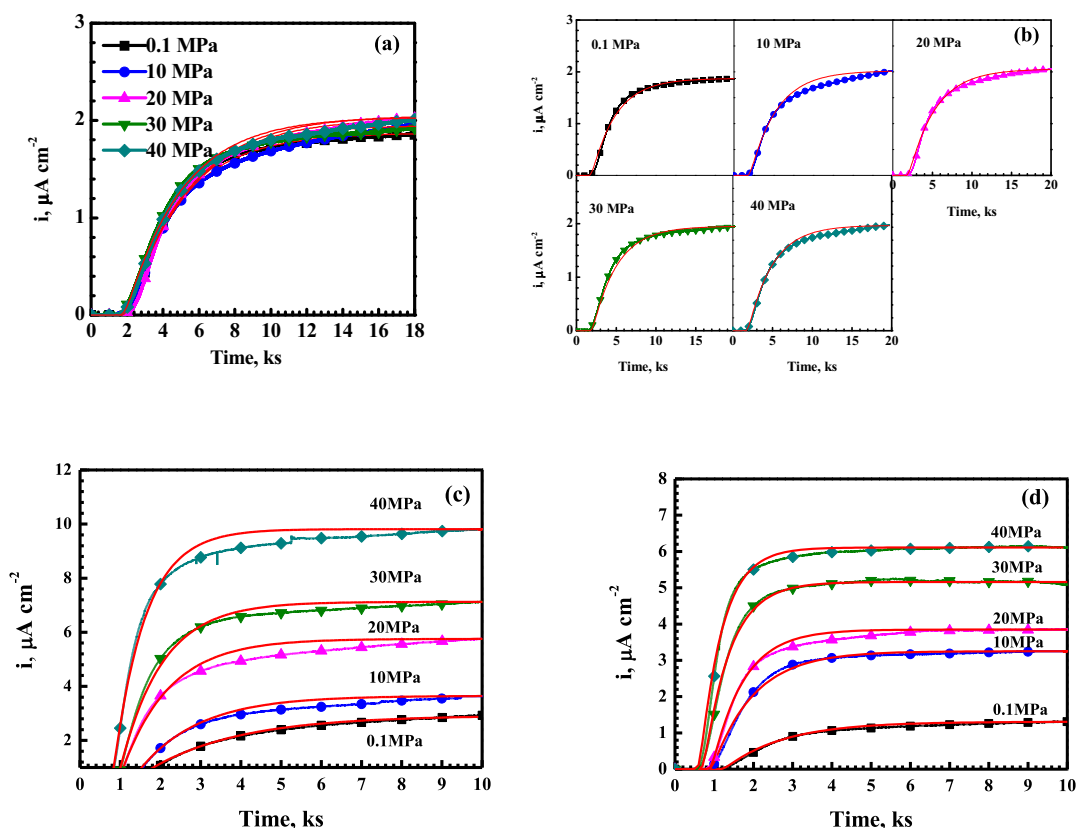
Fig. 2. Dependence of the hydrogen oxidation current density on time for different hydrostatic pressures at 25 °C: (a) and (b) group I specimens with the thickness of 1.1 mm and 100 nm Ni coated at the hydrogen exit side of specimens, (c) group II specimens with the thickness of 0.5 mm and 100 nm Ni coated at the hydrogen exit side of specimens and (d) group III specimens with the thickness of 0.5 mm and 100 nm Ni coated at both sides of specimens. The point plot denote experimental data, and the red lines fit the experimental data ((b) is a detail of (a)).

k increase with hydrostatic pressure for the 0.5 mm specimens, as shown in Fig. 3(c) and (d). Increasing k_p induces directly proportional increase in i_∞, although the increase in k causes only a small decrease in i_∞. For example, if hydrostatic pressure increases from 0.1 to 40 MPa for the group II specimens, k increases from 133.59 nm/s to 413.21 nm/s, and the denominator of the i_∞ equation $\left(2 + kl/D\right)$ increases from 2.21 to 2.65, which means that i_∞ decreases by 17%. However, k_p increases from 67.72 pmol/cm^2 s for 0.1 MPa to 273.31 pmol/cm^2 s for 40 MPa, resulting in i_∞ increasing by 400%. For a thin specimen, increasing the hydrostatic pressure can decrease the surface energy barrier for hydrogen atom absorption and desorption processes, resulting in an increase in k and k_p, and then i_∞.

Based on Eq. (10), the permeation concentration is $C_0 = k_p/k$. For a thin sample, increasing the hydrostatic pressure increases k and k_p, but the increase in k_p is greater than in k, resulting in C_0 increasing with hydrostatic pressure, as shown in Fig. 4.

Additionally, the ratios of the drift velocities V_s/V_b of groups II and III specimens increase with the hydrostatic pressure, as shown in Fig. 5. If V_s/V_b is very small, such that V_s is much smaller than V_b, then hydrogen absorption and desorption are the controlling steps. In contrast, hydrogen diffusion in the bulk is the controlling step. Therefore, hydrostatic pressure causes the entire process more likely to be bulk diffusion-controlled.

Changes in the hydrostatic pressure cause changes in the ratio of the drift velocities and hence changes in the concentrations at

Table 1
Measured and calculated results for the three groups of specimens.

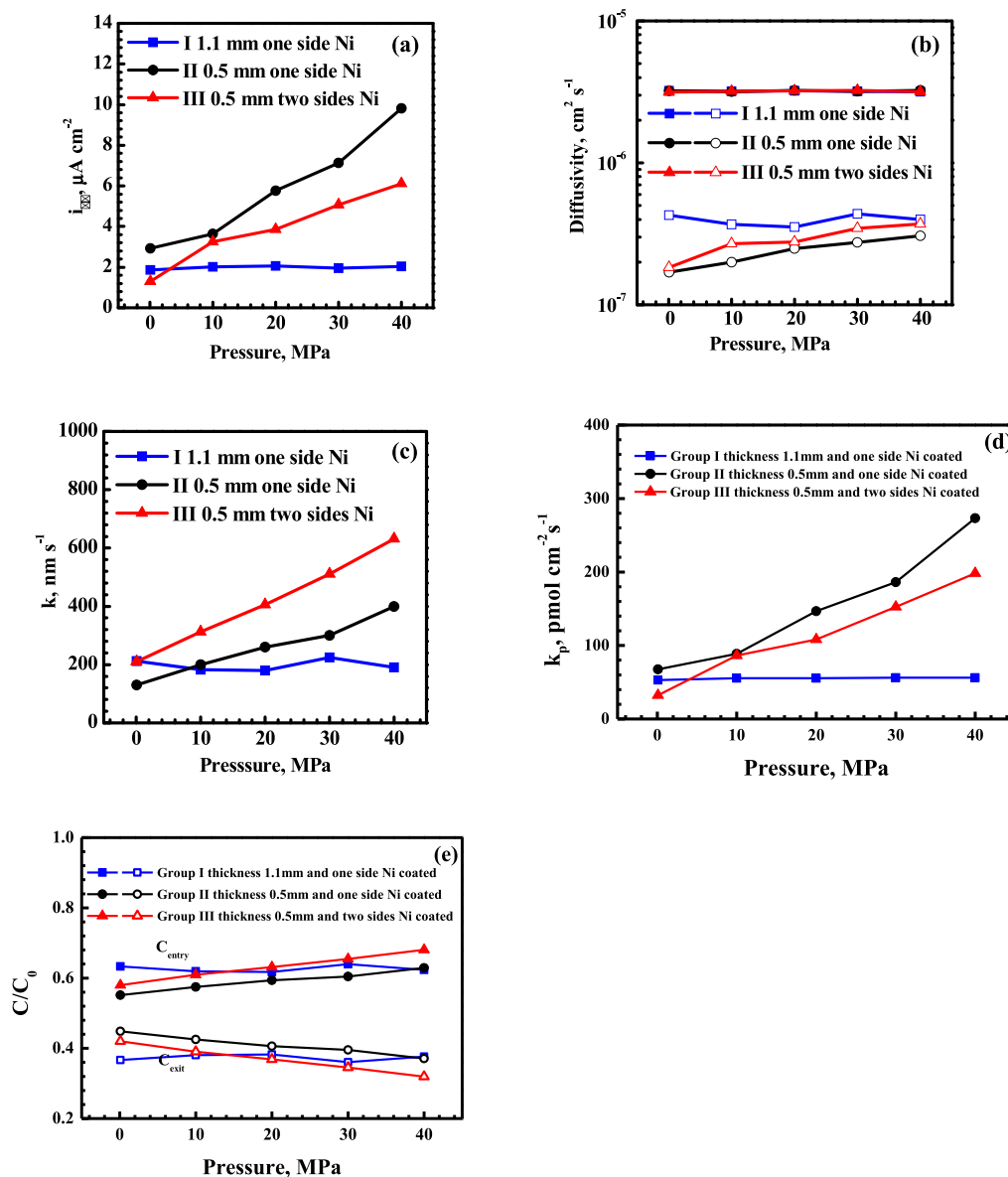| Specimen group	Pressure MPa	i_∞ μA/cm²	D 10⁻⁶ cm²/s	D_c 10⁻⁷ cm²/s	k nm/s	k_p pmol cm⁻² s⁻¹	C_0 μmol cm⁻³	C_{entry} μmol cm⁻³	C_{exit} μmol cm⁻³
	0.1	1.87	3.21	4.27	212.17	53.01	2.49	1.58	0.92
I	10	2.02	3.2	3.68	182.23	55.43	3.02	1.87	1.15
	20	2.05	3.23	3.52	179.89	55.44	3.08	1.9	1.18
	30	1.95	3.29	4.37	225.12	56.12	2.49	1.59	0.9
	40	2.04	3.18	3.98	190.34	56.09	2.95	1.84	1.11
	0.1	2.92	3.21	1.69	133.59	67.72	5.2	2.87	2.33
	10	3.64	3.18	2	200.12	88.75	4.44	2.55	1.89
II	20	5.76	3.25	2.48	262.22	147.23	5.56	3.35	2.29
	30	7.13	3.2	2.75	301.46	186.12	6.2	3.75	2.45
	40	9.81	3.24	3.06	413.21	273.31	6.83	4.3	2.53
	0.1	1.31	3.14	1.83	210.05	32.27	1.54	0.89	0.65
	10	3.25	3.2	2.7	311.76	86.31	2.77	1.69	1.08
III	20	3.85	3.22	2.77	406.21	108.14	2.67	1.68	0.98
	30	5.08	3.25	3.45	511.33	153.01	2.99	1.95	1.03
	40	6.11	3.18	3.7	631	198.23	3.14	2.14	1

Fig. 3. Variations of different parameters as functions of hydrostatic pressure for the three groups: (a) steady-state current density i_∞, (b) diffusivity D (solid) and D_c (hollow), (c) desorption rate k, (d) absorption parameter k_p, and (e) normalized hydrogen concentrations at the entry C_{entry}/C_0 (solid) and exit sides C_{exit}/C_0 (hollow).

the entry and exit sides. In Eq. (11), the normalized concentrations at the entry and exit sides are plotted in Fig. 6. For group II and III specimens permeation at 0.1 MPa, both normalized concentrations at the entry and exit sides are near 0.5 due to the small drift velocity ratios. As hydrostatic pressure increases, the ratio of the drift velocities increases, meaning that the normalized concentration approaches 1 at the entry side and 0 at the exit side. For example, at 0.1 MPa, normalized concentration for group II specimens is 0.55 and 0.45 at the entry and exit sides, respectively. However, at 40 MPa, normalized concentration at the entry and exit sides is 0.63 and 0.37, respectively. The phenomenon that i_∞ increases with hydrostatic pressure can be qualitatively explained. The boundary conditions are more ideal at high pressure, thus a large hydrogen concentration gradient appears in the bulk metal, which causes i_∞ to increase with hydrostatic pressure, as shown in Fig. 3(a).

4.2. Effect of hydrostatic pressure on diffusivity

As shown in Fig. 3(b), for the group II and III 0.5 mm thick specimens, D_c obtained from the classic model increases slightly with hydrostatic pressure, which is different from the previous work [12,13,15].

However, the intrinsic diffusivity D is almost independent of the hydrostatic pressure. As shown in Fig. 3(c), the desorption rate k, which depends on the surface conditions, increases with hydrostatic pressure. This means that the hydrostatic pressure does not influence the bulk diffusion, but does affect the surface reactions.

A large value of k means that there is a small energy barrier, which hydrogen atoms must overcome and that the bulk diffusion process plays an important role during permeation. Fig. 3(c) indicates that for the thin 0.5 mm specimens, the hydrostatic pressure increases k and reduces the surface energy barrier for hydrogen atoms involved in absorption and desorption processes. As surface energy barrier reduces, hydrogen atoms diffuse quickly through the
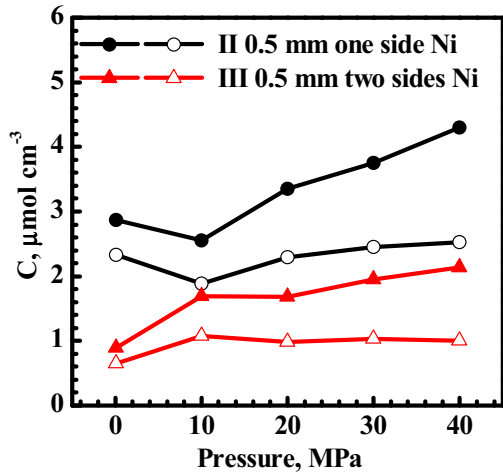
Fig. 4. Variation in hydrogen concentration on the surface for different hydrostatic pressure for groups II with the thickness of 0.5 mm and 100 nm Ni coated at the hydrogen exit side of specimens and III samples with the thickness of 0.5 mm and 100 nm Ni coated at both sides of specimens. The entry side is solid, the exit side is hollow.
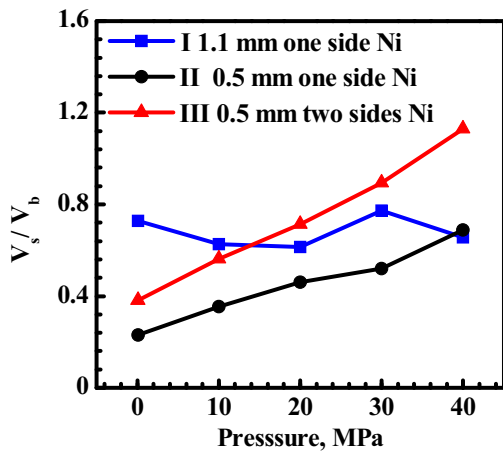

Fig. 5. Relationship between the drift velocity ratio V_s/V_b and hydrostatic pressure.
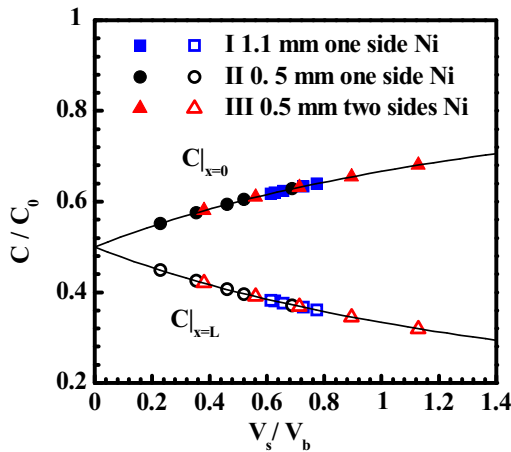

Fig. 6. Relationship between the normalized concentration and the drift velocity ratio V_s/V_b (solid line denotes theoretical prediction).

Table 2
Intrinsic diffusivity for low and high hydrostatic pressure.

Pressure MPa	$D_{ij}/10^{-6}$ cm²/s						D_i 10^{-6} cm²/s	D 10^{-6} cm²/s
	Group I		Group II		Group III			
≤10 MPa	3.21	3.2	3.21	3.18	3.14	3.2	3.19	3.2
≥30 MPa	3.2	3.18	3.2	3.24	3.25	3.18	3.21	

surface to the subsurface, and the total duration of hydrogen atoms moving from one side to the other side of the specimens reduces. Finally, the apparent diffusivity increases.

The single factor analysis model (SFAM) [30] was used to analyse the correlation between the hydrostatic pressure and the intrinsic diffusivity D. The rejection region, F, was calculated by:

$$F = \frac{S_A/f_A}{S_e/f_e} \tag{12}$$

where S_A and S_e are the sums of the squares of the standard deviations of the factor A and the error e, respectively. The variables f_A and f_e are the degrees of freedom of the factor A and the error e, respectively.

Data for the hydrostatic pressure less than 10 MPa and higher than 30 MPa are listed in Table 2.

As seen in Table 2, the error square sum is $S_e = \sum_{i=1}^{2}\sum_{j=1}^{6}\left(D_{ij} - \bar{D_i}\right)^2 = 0.0081$, the total declination square sum is $S_T = \sum_{i=1}^{2}\sum_{j=1}^{6}\left(D_{ij} - \bar{D}\right)^2 = 0.0091$, and the declination square sum for the hydrostatic pressure is $S_A = S_T - S_e = 0.0001$. The degrees of freedom are $f_T = 11$, $f_A = 1$, and $f_e = 10$. Thus, $F = 0.12$, and $= 4.96$ (95%) and $F_{0.01}(1,10) = 10.56$ (99%). Because F is less than $F_{0.05}$, the factor A, i.e., the hydrostatic pressure, has no influence on D. The mean and 95% confidence intervals based on the t distribution for all of the diffusivities is $(3.2 \pm 0.04) \times 10^{-6}$ cm²/s. D is independent of the thickness and surface conditions of the specimen. However, D_c based on the classic model is lower than D and depends on the thickness and surface conditions of the specimen. D_c for a thin specimen increases slightly with hydrostatic pressure.

4.3. Effect of specimen thickness on hydrogen permeation under hydrostatic pressure

For the group I specimens with 1.1 mm thickness and Ni coated exit side, D obtained from the Zhang's model has a mean value of 3.20×10^{-6} cm²/s, and D_c has a mean value of 3.96×10^{-7} cm²/s, listed in Table 1. The mean value of D for the group II 0.5 mm thick specimens with Ni coated exit side is 3.22×10^{-6} cm²/s. The mean value of D_c for group II specimens is 2.40×10^{-7} cm²/s, which is decreased compared with group I specimens. This phenomenon demonstrates the thickness effect on D_c obtained by the classic model [18,23,31]. D remains almost the same, meaning that the thickness effect on D_c is not due to the bulk diffusion, but is a result of the surface energy barrier [18].

For the 1.1 mm thick group I specimens, the variations in the parameters i_∞, D, D_c, k, k_p, and C_0 as functions of the hydrostatic pressure are irregular and are similar to the Elhamid's work [19]. Elhamid stated that for the specimens thicker than 1 mm, bulk diffusion, rather than surface effects, dominates hydrogen permeation. As shown in Fig. 5, group I specimens are thicker than group II specimens, so the ratio of the drift velocities for group I specimens is greater than that for group II specimens at hydrostatic pressure less than 30 MPa, which means that bulk diffusion is more likely
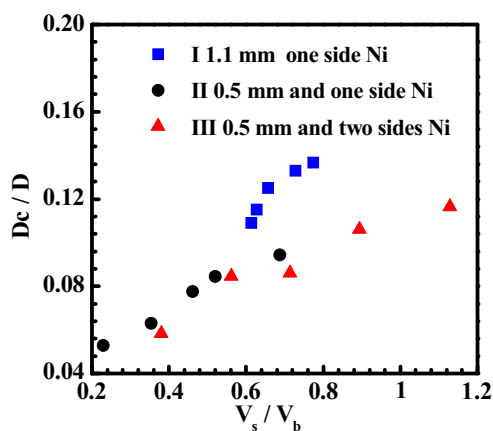
Fig. 7. Relationship between the normalized diffusivity and the drift velocity ratio V_s/V_b.

to be the controlling step in the permeation processes of group I specimens.

Fig. 6 shows that the normalized concentrations of group I specimens are more idealised than those of group II because of a greater ratio of drift velocities. Fig. 7 indicates that the difference in the diffusivities determined from the two models decreases with the specimen thickness. However, even for the 1.1 mm thick group I and II specimens, the diffusivity value calculated by the classic model is still much smaller than the Zhang's model. The appropriateness of the classic model can be gauged by the ratio of the drift velocity through the surface to that in the bulk. The normalized diffusivity, D_c/D, for all of the specimens in group I is a function of the ratio of drift velocities, which is higher than in group II specimens with the same surface conditions.

4.4. Effect of nickel coating on hydrogen permeation

Comparing group II and III specimens in Table 1, one can see that nickel coating at the entry side clearly influences hydrogen permeation. For the group III 0.5 mm thick specimens with two Ni coated sides, D has a mean value of 3.20×10^{-6} cm²/s, which is almost the same as for group II specimens. The mean value of D_c is 2.89×10^{-7} cm²/s, which increases slightly compared with group II specimens. This means that the 100 nm nickel coating at the entry side can increase D_c. According to Fig. 3(c) and (d), nickel coating increases the value of k and decreases the value of k_p, meaning that nickel reduces the energy barrier at the entry side and decrease the amount of absorbed hydrogen atoms at the same time. Based on Eq. (9), $i_\infty = k_p F/\left(2 + kl/D\right)$, the combined action of k and k_p induces a decrease of steady-state current density i_∞.

Based on Eq. (10), hydrogen concentration of group III specimens at the entry side is smaller than group II specimens in Fig. 4. The ratio of drift velocity for group III specimens is slightly higher than for group II, meaning that the normalized concentration of group III specimens is more idealised, shown in Figs. 5 and 6. Thus, hydrogen diffusion in the bulk metal is more likely to be a rate-determining step in group III rather than group II specimens.

5. Conclusions

The influence of surface hydrogen absorption and desorption under hydrostatic pressure on hydrogen diffusivity is quantified. Taking surface effects of hydrogen permeation into account, the intrinsic diffusivity D of the A514 steel is $(3.2 \pm 0.04) \times 10^{-6}$ cm²/s, which is independent of the sample thickness and surface conditions, as well as the hydrostatic pressure. However, the apparent

diffusivity D_c based on the classic model is much smaller than D and depends on the thickness and surface conditions of the sample, and increases slightly with hydrostatic pressure for thin specimens.

For a thin specimen, the steady-state current density i_∞ and surface hydrogen concentration increase with hydrostatic pressure because hydrostatic pressure can decrease the energy barrier for hydrogen atom absorption and desorption processes, which increases both the adsorption parameter k_p and the desorption rate k, although the increase is more evident for k_p.

References

[1] T.S. Taylor, T. Pendlington, R. Bird, Foinaven super duplex materials cracking investigation, Houston, Texas, in: Offshore Technology Conference, 10965, 1999.
[2] L.P.M. Santos, M. Béreš, I.N. Bastos, S.S.M. Tavares, H.F.G. Abreu, M.J. Gomes da Silva, Hydrogen embrittlement of ultra high strength 300 grade maraging steel, Corros. Sci. 101 (2015) 12–18.
[3] I.-J. Park, S. -m. Lee, H. -h. Jeon, Y.-K. Lee, The advantage of grain refinement in the hydrogen embrittlement of Fe–18Mn–0.6C twinning-induced plasticity steel, Corros. Sci. 93 (2015) 63–69.
[4] F.J. Recio, M.C. Alonso, L. Gaillet, M. Sánchez, Hydrogen embrittlement risk of high strength galvanized steel in contact with alkaline media, Corros. Sci. 53 (2011) 2853–2860.
[5] G. Wang, Y. Yan, J. Li, J. Huang, Y. Su, L. Qiao, Hydrogen embrittlement assessment of ultra-high strength steel 30CrMnSiNi2, Corros. Sci. 77 (2013) 273–280.
[6] R. Nishimura, J. Shirono, A. Jonokuchi, Hydrogen-induced cracking of pure titanium in sulphuric acid and hydrochloric acid solutions using constant load method, Corros. Sci. 50 (2008) 2691–2697.
[7] W.W. Wang, Y.J. Su, Y. Yan, J.X. Li, L.J. Qiao, W.Y. Chu, X.K. Wang, Y. Xing, The role of hydrogen in stress corrosion cracking of 310 austenitic stainless steel in a boiling MgCl2 solution, Corros. Sci. 60 (2012) 275–279.
[8] P. Woollin, Hydrogen embrittlements stress corrosion cracking of superduplex stainless steel, Corrosion (2001) 01018.
[9] X.S. Du, Y.J. Su, J.X. Li, L.J. Qiao, W.Y. Chu, Stress corrosion cracking of A537 steel in simulated marine environments, Corros. Sci. 65 (2012) 278–287.
[10] S. Olsen, S.M. Hesjevik, Hydrogen embrittlement from CP on supermartensitic stainless steels – recommendations for new qualification methods, Corrosion (2004) 04546.
[11] J. Woodward, R.P.M. Procter, The effect of hydrostatic pressure on hydrogen permeation and embrittlement of structural steels in seawater, Conf. Proc. (1996) 253–267.
[12] Leonard Nanis, J.J. DeLuccia, Effects of hydrostatic pressures on electrolytic hydrogen in iron, american society for testing and material, ASTM STP 445 (1969) 55–67.
[13] A. Smirnova, R. Johnsen, Influence of temperature and hydrostatic pressure on hydrogen diffusivity and permeability in 13%Cr super martensitic stainless steel under cathodic protection corrosion, Corrosion 10292 (2010).
[14] R.F. Blundy, L.L. Shreir, Permeation of hydrogen through fe during cathodic polarization under hydrostatic pressure, Philos. Mag. 20 (1969) 1177–1187.
[15] R.F. Blundy, L.L. Shreir, The effect of pressure on the permeation of hydrogen through steel, Corros. Sci. 17 (1977) 509–527.
[16] E. Bender, U. Klein, W.P. Schmitt, J.M. Prausnitz, Thermodynamics of gas solubility: relation between equation-of-state and activity-coefficient models, Fluid Phase Equilib. 15 (1984) 241–255.
[17] M.A.V. Devanathan, Z. Stachurski, The mechanism of hydrogen evolution on iron in acid solutions by determination of permeation rates, J. Electrochem. Soc. 111 (1964) 619–623.
[18] T.Y. Zhang, Y.P. Zheng, Effects of absorption and desorption on hydrogen permeation—I. Theoretical modeling and room temperature verification, Acta Mater. 46 (1998) 5023–5033.
[19] M.H.A. Elhamid, B.G. Ateya, H.W. Pickering, Determination of the rate constants of hydrogen absorption into metals, J. Electrochem. Soc. 147 (2000) 2959–2963.
[20] T. Zakroczymski, Adaptation of the electrochemical permeation technique for studying entry, transport and trapping of hydrogen in metals, Electrochim. Acta 51 (2006) 2261–2266.
[21] P. Castaño Rivera, V.P. Ramunni, P. Bruzzoni, Hydrogen trapping in an API 5L X60 steel, Corros. Sci. 54 (2012) 106–118.
[22] J.J.M. Jebaraj, D.J. Morrison, I.I. Suni, Hydrogen diffusion coefficients through Inconel 718 in different metallurgical conditions, Corros. Sci. 80 (2014) 517–522.

[23] S. Wach, A.P. Miodownik, J. Mackowiak, The diffusion of hydrogen through pure iron membranes, Corros. Sci. 6 (1966) 271–285.
[24] R.N. Iyer, H.W. Pickering, Analysis of hydrogen evolution and entry into metals for the discharge-recombination process, J. Electrochem. Soc. 136 (1989).
[25] R.N. Iyer, H.W. Pickering, Construction of iso-Coverage tafel plots to evaluate the HER transfer coefficient, J. Electrochem. Soc. 137 (1990) 3512–3514.
[26] R.N. Iyer, H.W. Pickering, Mechanism and kinetics of electrochemical hydrogen entry and degradation of metallic systems, Mater. Sci. 20 (1990) 299–338.
[27] J.-S. Wang, On the diffusion of gases through metals, Math. Proc. Cambridge Philos. Soc. 32 (1936) 657–662.

[28] J. Svoboda, G. Mori, A. Prethaler, F.D. Fischer, Determination of trapping parameters and the chemical diffusion coefficient from hydrogen permeation experiments, Corros. Sci. 82 (2014) 93–100.
[29] S.J. Kim, D.W. Yun, H.G. Jung, K.Y. Kim, Determination of hydrogen diffusion parameters of ferritic steel from electrochemical permeation measurement under tensile loads, J. Electrochem. Soc. 161 (2014) 8.
[30] H. Ma, C. Cui, X. Li, Z. Sun, Study of high performance autoclaved shell-aggregate from propylene oxide sludge, Constr. Build. Mater. 25 (2011) 3030–3037.
[31] J. L.N.a.W.B, A. McBreena, Method for determination of the permeation rate of hydrogen through metal membranes, Electrochem. Soc. 113 (1966) 1218–1222.